JOURNAL OF QUATERNARY SCIENCE (2022) **37**(3) 478–488 ISSN 0267-8179. DOI: 10.1002/jqs.3394

JQS Journal of Quaternary Science QRA Quaternary Research Association

Modelling climate constraints on the formation of pluvial Lake Bonneville in the Great Basin, United States

BRYCE K. BELANGER,[1,2]* WILLIAM H. AMIDON,[1] BENJAMIN J. C. LAABS,[3] JEFFREY S. MUNROE[1] and BRENDON J. QUIRK[4,5]

[1]Department of Geology, Middlebury College, Middlebury, VT, USA
[2]Department of Earth and Environmental Sciences, Vanderbilt University, Nashville, TN, USA
[3]Department of Geosciences, North Dakota State University, Fargo, ND, USA
[4]Department of Geology and Geophysics, University of Utah, Salt Lake City, UT, USA
[5]Department of Geosciences, University of Massachusetts, Amherst, MA, USA

Received 25 March 2021; Revised 18 October 2021; Accepted 21 October 2021

ABSTRACT: This study uses a hydrologic-balance model to evaluate the range of precipitation and temperature (P-T) conditions required to sustain Lake Bonneville at two lake levels during the late Pleistocene. Intersection with a second set of P-T curves determined from glacial modelling in the nearby Wasatch Mountains places tighter climatic constraints that suggest gradually increasing wetness from ~21 to 15 ka. Specifically, during the latter part of the Last Glacial Maximum (LGM) (~21–20 ka), Lake Bonneville approached its highest level under conditions roughly 9.5°C colder but only 7% wetter than modern. As the lake reached its pre-flood Bonneville level (~18.2–17.5 ka), climate conditions were ~16% wetter and ~9°C colder than modern. By *ca.* 15–14.8 ka, Lake Bonneville abandoned the overflowing Provo level under conditions that were ~21% wetter and ~7°C cooler. These results suggest that regional LGM highstands were not caused by large increases in precipitation, but rather by a climatic optimum in which moderate wetness combined with depressed temperatures to create a positive hydrologic budget. Later highstands during Heinrich I from 17 to 15 ka were likely achieved under gradual increases in precipitation, prior to a transition to drier conditions after 15 ka. © 2021 John Wiley & Sons, Ltd.

KEYWORDS: Great Basin; Lake Bonneville; Last Glacial Maximum; pluvial lakes; water-balance modelling

Introduction

Freshwater availability is a concern in the southwestern United States, where natural changes in temperature and precipitation over the last 30 000 years have resulted in dramatic fluctuations of this resource. Climate models predict that continued climate change will cause dry regions like the southwestern United States to become even drier (e.g. Cook *et al.*, 2015; Cook *et al.*, 2020; Seager and Vecchi, 2010), leading to increased aridity and reduced freshwater availability. Significant runoff declines are anticipated across western North America even under the most conservative estimates of warming, and the risk of extreme drought across the region is expected to increase by over 100% before the end of the 21st century (Cook *et al.*, 2020; Hatchett, 2018). Accordingly, there is an immediate need for accurate models of future precipitation in the southwestern United States, which benefits from benchmarking with reliable estimates of past and present terrestrial water balance. To this end, this study employs water-balance modelling to constrain palaeoclimate conditions during two late Pleistocene stages of pluvial Lake Bonneville in the Great Basin of the southwestern United States (Fig. 1). While similar reconstructions already exist (Ibarra *et al.*, 2019; Matsubara and Howard, 2009), this study explores the robustness of these results by using a different methodology (Condom *et al.*, 2004) and integrating it with a highly refined alpine glacial chronology (Quirk *et al.*, 2020).

Former high levels of Lake Bonneville are recorded by the presence of beaches, deltas, wave-cut platforms and other landforms (Gilbert, 1890). The spatial distribution of these features reveals the extent of the ancient lake and dating of these landforms and other intrabasinal deposits constrains the timing of past fluctuations in lake area. Most pluvial lakes in the Great Basin of the western United States reached their maximum extents between 21 000 and 15 000 years ago (21–15 ka) (Benson *et al.*, 1990; Hudson *et al.*, 2019; Munroe and Laabs, 2013b) during the latter part of the global Last Glacial Maximum (LGM) and the early part of subsequent deglaciation. Lake Bonneville was the largest pluvial lake in the region, filling a series of extensional-tectonic basins including the basin occupied by the modern Great Salt Lake. Bonneville was dominantly fed by the Bear, Weber and Provo Rivers draining from the Wasatch and Uinta mountain ranges, and the Sevier and Beaver Rivers in west-central Utah (Oviatt, 2015). Lake Bonneville had a maximum surface area in excess of 50 000 km^2 (Hostetler *et al.*, 1994; Oviatt, 2015). The late Pleistocene chronology of the lake is known from numerous studies, primarily based on radiocarbon dating of carbonates and organic matter preserved in lacustrine sediment (e.g. Broecker and Kaufman, 1965; Currey and Oviatt, 1985; Currey, 1990; Godsey *et al.*, 2005; Scott *et al.*, 1983), tephrastratigraphy of intrabasinal deposits (Miller *et al.*, 2008; Oviatt and Nash, 1989; 2014), palaeomagnetic properties of lake sediment (Benson *et al.*, 2011) and uranium-series dating of cave carbonates (McGee *et al.*, 2012), as summarised by Oviatt (2015). The last major transgression of Lake Bonneville began at *ca.* 29 ka, and was interrupted by notable oscillations in elevation (Oviatt, 1997). The transgression spanned at least 10 000 years and included a brief (centuries or less) occupation of the prominent Stansbury shoreline (1380 m above sea level (asl)) at *ca.* 25 ka

*Correspondence: B. K. Belanger, as above.
E-mail: bryce.k.belanger@vanderbilt.edu

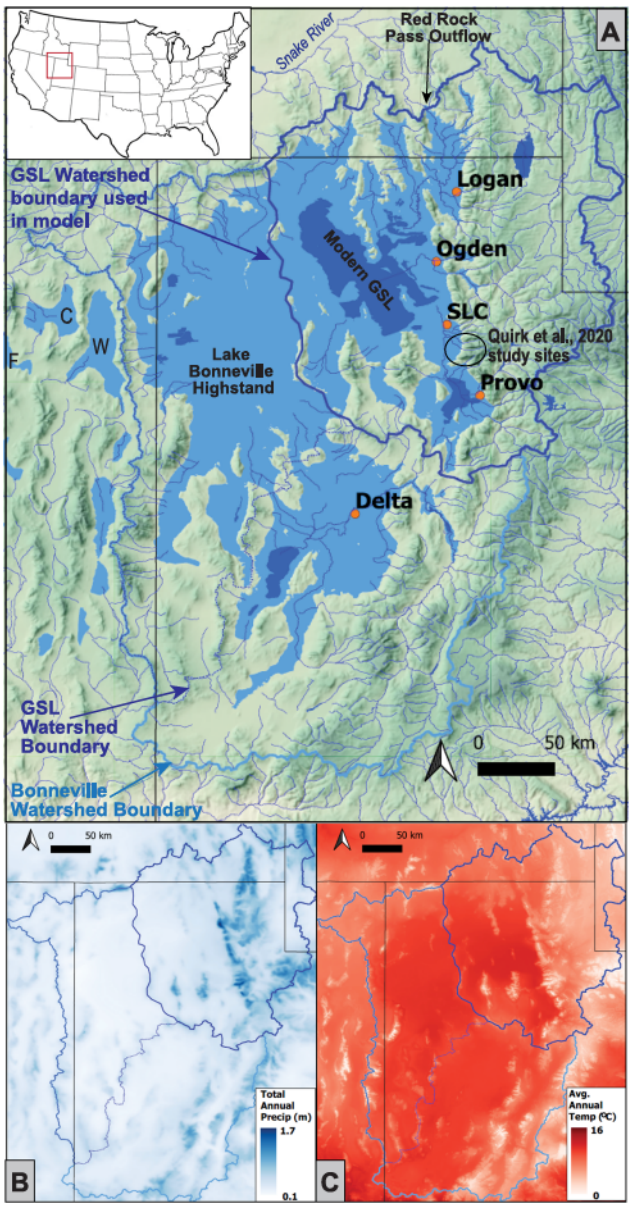

Figure 1. A) Map of Lake Bonneville at its highest extent, along with pluvial lakes Franklin (F), Clover (C) and Waring (W) (Reheis, 1999). Modern lake locations are shown in dark blue. The altered watershed of the Great Salt Lake (GSL) accounts for regions to the west and south that are within the physical GSL watershed, but are not a source of surface inflow or groundwater recharge to the GSL (White *et al.*, 2014). Pan evaporation and weather data for this study were obtained from stations in Logan, Ogden, Salt Lake City (SLC), Provo and Delta. B) Total annual precipitation over the study area derived by summing the monthly PRISM grids. C) Mean annual temperature derived by averaging the monthly PRISM grids. [Color figure can be viewed at wileyonlinelibrary.com]

(Oviatt*et al.*, 1990). The lake continued to rise in its topographically closed basin, undergoing at least three subsequent oscillations at *ca.* 22, 21 and 19 ka (Oviatt, 1997), before reaching a maximum elevation of 1550 m asl where it began to overflow, marked by the prominent Bonneville shoreline.

Although some studies have proposed that Lake Bonneville overflowed for a period of hundreds of years or longer (Pack, 1939; Williams, 1952), Oviatt and Jewell (2016) report widespread geomorphic evidence supporting the inference of G.K. Gilbert (1890) that the Bonneville shoreline was occupied only briefly before catastrophic failure of the sill at its overflow point resulted in a 110 m drop in water surface elevation at *ca.* 18.2 ka (Lifton *et al.*, 2015; O'Connor, 1993; 2016). The lake then stabilised and began to overflow at 1440–1450 m asl, forming the prominent Provo shoreline, which is marked by nearshore deposits and broad wave-cut platforms throughout the Bonneville basin. Although numerous radiocarbon ages limit the time when the Provo shoreline was occupied to 18.2–14.8 ka (Godsey *et al.*, 2005; Miller *et al.*, 2013), it is unclear whether overflow was continuous during this time (Miller, 2016). After *ca.* 14.8 ka, Lake Bonneville regressed and abandoned the Provo shoreline, presumably due to a warmer and drier climate in the Lake Bonneville basin (Godsey *et al.*, 2011), and reached an elevation near the modern Great Salt Lake by *ca.* 13 ka (Oviatt, 2015). Despite the apparent exactness of this chronology, we acknowledge that none of these events is known with century or sub-century precision. Hereafter we use '*ca.*' to denote events whose analytical precision suggests that timing is known with sub-millennial resolution, but for which significant systematic uncertainties remain.

As the largest of the Great Basin pluvial lakes, Lake Bonneville's rise and fall is a critical recorder of regional hydrologic change in the Great Basin. This study focuses on constraining the climatic conditions responsible for the formation of this lake. Specifically, by combining a hydrologic model with previous results from energy-balance modelling of nearby glaciers, we are able to estimate the factors by which temperature (T) decreased and precipitation (P) increased (relative to modern) at the times when the Bonneville and Provo shorelines were occupied. We first use modern climate data to calibrate an evaporation model for the Lake Bonneville basin. We then use this regionally calibrated evaporation model within the hydrologic balance approach developed by Condom *et al.* (2004) to generate two sets of P-T changes that could have sustained the lake at the Bonneville and Provo levels. Finally, we intersect these P-T estimates with those derived from glacier reconstructions in the nearby Wasatch Mountains to provide tighter constraints on palaeoclimate conditions in this region (Quirk *et al.*, 2020). Our results provide evidence against the idea that large increases in precipitation drove lake transgressions during the LGM (e.g. Antevs 1948; Hostetler and Benson 1990), and instead suggest that colder temperatures combined with reduced summer evaporation enabled the rise of Lake Bonneville from 22 to 18 ka.

Methods

Water-balance model overview

This study employs a modified version of the lumped water-balance model developed by Condom *et al.* (2004) and is implemented here in MATLAB. At the biggest scale, this model computes evaporative losses from the lake and watershed as a function of temperature and radiation and attempts to balance them against precipitation inputs. This is expressed mathematically as:

$$dZ/dT = 0 = P - (E_{Lake} + Et_{ws}) \quad (1)$$

where dZ/dT denotes change in lake surface elevation over time, P is precipitation rate (mm/month), Et_{ws} is evapotranspiration rate from the land surface (mm/month), and E_{Lake} is evaporation rate from the lake surface (Condom *et al.*, 2004).

The two evaporation terms (E_{lake} and Et_{ws}) are computed from standard evaporation equations, of which many have been proposed in the literature (see review by Xu and Singh, 2000). These are all empirically derived radiation-based equations that are very similar in form and have been shown to have

good predictive power across a range of climatic settings. Because we have no *a priori* reason to choose one over the other, we first compare the ability of three standard evaporation equations (Abtew, 1996; Turc, 1961; Condom *et al.*, 2004) to predict observed pan evaporation (Western Regional Climate Center, 2019) at five sites throughout the Bonneville basin (Salt Lake City, Provo, Logan, Ogden and Delta, Utah; Fig. 1). These stations were selected for their location and data availability, but also represent a wide range in mean monthly temperature (-4.5 to 26°C) and precipitation (8–72 mm/month). Data from these stations are recorded as monthly sums or averages, and evaporation is not measured during winter months when temperatures are commonly below freezing.

The Abtew (1996) equation models potential evaporation as a function of solar radiation and a location-specific calibration factor:

$$EP = K \times (Rg/\lambda) \tag{2}$$

where EP is potential evaporation (mm day^{-1}), Rg is total solar radiation (MJ m^{-2} day^{-1}), λ is latent heat (MJ kg^{-1}), and K is a unitless coefficient used as a calibration factor.

The Turc (1961) equation includes an additional temperature term:

$$EP = K \times (T/T + 15) \times (Rg + 50) \tag{3}$$

where EP is potential evaporation (mm day^{-1}), T is air temperature (°C) and Rg is solar radiation (cal cm^{-2} day^{-1}).

Finally, the Condom *et al.* (2004) model is derived from Xu and Singh (2000) and Hargreaves (1975) and uses the same variables as the Turc model in a different formulation:

$$EP = (Rg/\lambda) \times (T + 17.8) \times K \tag{4}$$

where EP is potential evaporation (mm day^{-1}), Rg is the total solar radiation (in J cm^{-2} day^{-1}), T is air temperature (°C), and λ is latent heat (Cal/g), calculated here as:

$$\lambda = 595 - 0.51T \tag{5}$$

All of these models include a location-specific coefficient K, which must be locally calibrated, which poses a unique challenge in the Bonneville basin because of the immense watershed of Lake Bonneville at its highest level. We approach this problem by optimising K at each of the five pan evaporation locations mentioned above and averaging the values to produce a single calibration factor representative of the basin as a whole. This process is illustrated graphically in Fig. 2. The first step is to multiply observed pan evaporation at each station by a coefficient of 0.75 to account for the enhanced evaporation from a pan relative to water from the soil or lake surface. A factor of 0.75 was selected based on recommendation from the Task Committee on Hydrology Handbook (1996) for pan evaporation calibration in this region. The second step is to identify the best-fit K value for each evaporation model at each station by minimising the sum of the squared residuals (SSR) between observed and model-predicted pan evaporation for a 12-month year at that station (i.e., 12 residuals). Monthly 'at station' evaporation is computed using mean monthly insolation, which is calculated from hourly total direct and diffuse solar radiation data from the National Solar Radiation Database 1991–2010 (Sengupta *et al.*, 2018) and mean temperature values from weather station data at the station of interest (data archived by the Western Regional Climate Center). Finally, station-specific SSR and K values are averaged to create single SSR and K values for each evaporation model (Fig. 2).

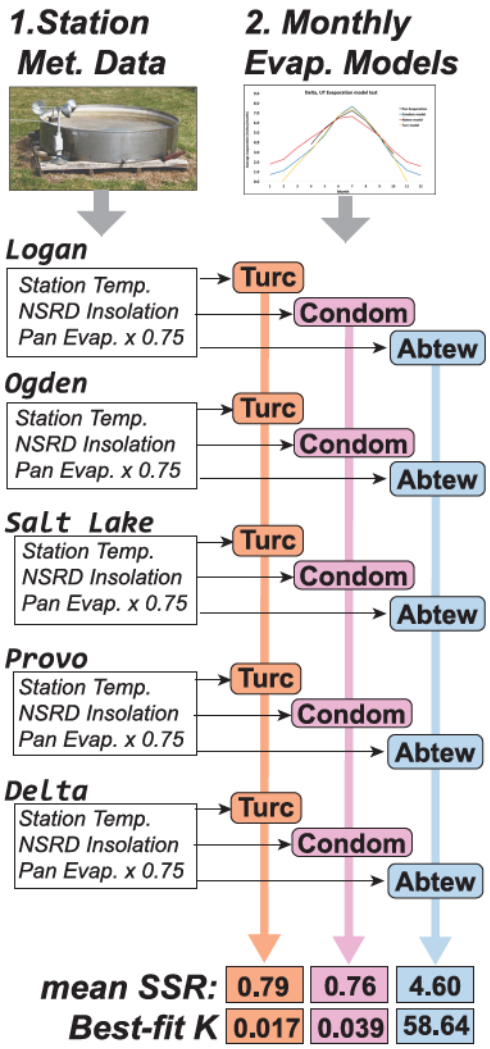

Figure 2. Schematic diagram showing the process used to determine the optimal evaporation coefficient (K). Station data from five stations were fed into three different monthly evaporation models and a best-fit value for K was determined for each of the 15 combinations by minimising the monthly SSR. The mean SSR and K values were then computed for each model, with the Condom model providing the best overall fit. [Color figure can be viewed at wileyonlinelibrary.com]

One potential issue with this approach is that stations available for calibration of the evaporation parameter K are located within a relatively restricted part of the Lake Bonneville watershed. Nonetheless we argue that the evaporation coefficient can reliably be applied to the broader watershed for a few reasons. First, the simple radiation-based evaporation model used in this study has been shown to be robust across a wide range of climatic settings (Xu and Singh, 2000). Second, given the temperature seasonality at the weather stations, the evaporation equations are calibrated on monthly mean temperatures that span roughly -4.5 to 26°C, encompassing the full above-freezing temperature range of the study area. Finally, the vast majority of the Bonneville basin is sparsely vegetated, conditions under which pan evaporation should be a good predictor of actual evaporation.

Model implementation

The main inputs to our lumped hydrologic model are four raster datasets representing: 1) modern monthly precipitation; 2) temperature; 3) radiation; and 4) a coded raster delineating lake or watershed pixels. Temperature and precipitation inputs are taken from 30-year normal (1981–2010) datasets

produced by the PRISM group (http://www.prism.oregonstate.edu/normals/) and solar insolation data from the Fick and Hijmans (2017) WorldClim 2 dataset. The former has a spatial resolution of 800 m, while the latter was down-sampled from 1000 m using bilinear interpolation to match the native resolution of the PRISM data.

The PRISM and WorldClim 2 raster data are similar to location-specific temperature (WRCC) and radiation (NSRD) datasets used in the calibration of K at the five cities where potential evaporation calibrations were made. For example, at Salt Lake City, the average PRISM temperature for the months of June, July and August is 23.26°C, while the station-specific mean temperature for this period is 23.68°C. Raster and station-specific insolation data are also similar, varying by approximately 5% annually for Salt Lake City. Thus, we do not consider the use of both meteorological and raster data in this study to be a cause for concern.

An additional model input called 'DT_lake' is used to adjust lake temperature for the offset between air and water temperature, thus allowing lake evaporation to occur at a water temperature colder or warmer than the air. DT_lake is computed monthly using observed differences between the air and Great Salt Lake surface temperatures from 1994 to 2006 from Belovsky *et al.* (2011).

Another consideration is that during Bonneville's highest levels *ca.* 18.4 ka, summer (June, July, August) top-of-atmosphere insolation was reduced by 5% from modern, whereas winter (December, January, February) was increased by 5% (Laskar *et al.* 2004). Likewise for the Provo level at *ca.* 14.8 ka, summer palaeo-insolation is reduced by 2.5% from modern while winter palaeo-insolation is increased by 2.5%. However, it is likely that the months in which 'summer' occurred would have shifted to match the months that were receiving maximum insolation at *ca.* 18.4 and 14.8 ka, respectively. In other words, 'summer' and 'winter' would have taken place during different segments of Earth's orbital ellipse than they do today. If the seasons perfectly followed shifting insolation, there would be no need to adjust insolation in the Bonneville or Provo model simulations. On the other hand, if the seasons did not shift at all in response to insolation, it would be warranted to apply the relevant increase or reduction in insolation to the Bonneville and Provo simulations. In our preferred simulation we have chosen not to adjust the palaeo-insolation, instead using modern insolation values and applying a 10% (2σ) uncertainty to them.

The Condom *et al.* (2004) model used in this study is a lumped equilibrium model that does not track changes in lake size over time, but instead seeks to identify the climatic conditions that allow precipitation inputs to match evaporative outputs assuming a specific lake extent (Fig. 3). Although the model sums water inputs and losses from pixels across the 2D watershed, the hydrologic balance is essentially a 1D calculation in which total precipitation inputs are balanced against total evaporative losses. In addition to precipitation and temperature, the major hydrologic variable in the model is soil water capacity (CapaS), which is first calibrated for a modern lake watershed using modern P and T values (stage 1), and then used as a 'known' input to constrain past P-T combinations required to sustain a palaeolake in the same watershed (stage 2). In this study the Great Salt Lake represents the modern lake (stage 1), whereas Lake Bonneville at the Bonneville and Provo shorelines represent the two palaeolakes that were modelled (stage 2).

In physical terms, CapaS can be thought of as the maximum amount of water (in mm) capable of being retained in the basin soil at any given time, with any excess running off into the lake. Thus, the first stage of any model run is an iterative search for the value of CapaS that achieves a hydrologic balance for the modern Great Salt Lake (1281 m asl – historic average surface elevation from 1847 to 1986). In each iterative cycle the hydrologic precipitation, evaporation and runoff are computed for each pixel over 120 sequential monthly time steps (10 years), enough to allow model spin-up and guarantee model stability under various conditions (Fig. 3). Runoff from land surface pixels is determined by tracking the water depth in each pixel (H_{ws}). During each time step, precipitation is first added to the pixel. If the mean monthly temperature is below freezing no evaporation occurs and H_{ws} is increased accordingly. If the temperature is above freezing and if the soil is not overflowing (resultant $H_{ws} <$ CapaS) then evapotranspiration (ET_{ws}) is estimated as:

$$ETws_{n+1} = (Hws_n/\text{CapaS}) \times (2 - (Hws_n/\text{CapaS})) \times EP_{n+1}. \quad (6)$$

If the soil is overflowing after adding precipitation ($H_{ws} >$ CapaS) then the question arises as to how much of the excess to make available for evaporation versus how much to runoff. We deal with this by invoking a variable termed the evaporation fraction (efract) which specifies what fraction of a month's potential evaporation should be removed prior to runoff with the remaining evaporation occurring after runoff has lowered H_{ws} to equal CapaS. For steps in which soil water (H_{ws}) exceeds CapaS by more than potential evaporation (EP), runoff and water level are then computed as:

$$\text{runoff}_n = (Hws_n - \text{CapaS}) - (EP_n \times \text{efract}) \quad (7)$$

$$Hws_{(n+1)} = Hws_n - \text{runoff}_n - EP_n \quad (8)$$

For example, if the monthly precipitation input causes H_{ws} to initially exceed CapaS by 10 mm, and monthly potential evaporation (EP) is 4 mm, then an efract value of 0.5 would allow 2 mm to be evaporated prior to runoff, allow the

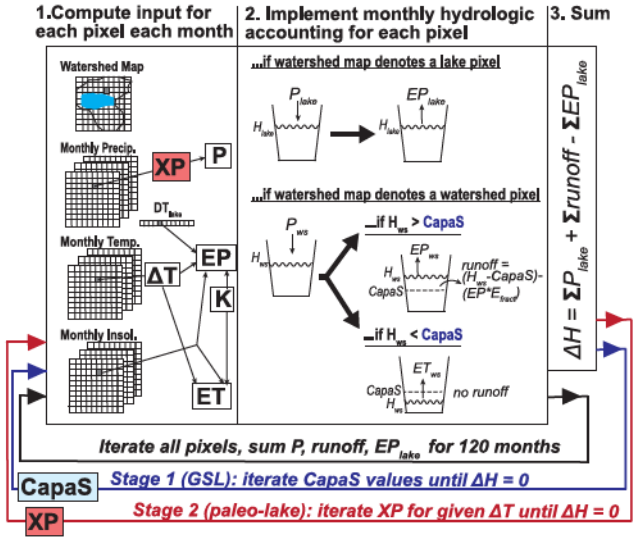

Figure 3. Schematic diagram showing how the hydrologic balance model works. Stage 1 uses the extent of the modern Great Salt Lake and modern precipitation, temperature and radiation data to calibrate soil water capacity (CapaS). Stage 2 uses the resultant CapaS value as an input to determine the various values of P and T required to balance incoming precipitation against outgoing evaporation for the known extents of Lake Bonneville at the Bonneville and Provo stages. [Color figure can be viewed at wileyonlinelibrary.com]

remaining 8 mm to runoff, and then apply another 2 mm of evaporation after runoff, leaving H_{ws} 2 mm below CapaS.

After a single iteration (120 monthly time steps), the model aggregates total runoff and evaporation across all pixels and equates them with cumulative precipitation to assess whether a positive or negative hydrologic balance has been achieved. MATLAB's fzero function is then used to iteratively solve for a CapaS value that yields a net hydrologic budget of zero, such that total runoff and evaporative losses are equal.

In the second stage, the model is run using the CapaS value determined in stage 1 as an input, this time performing an iterative search for a precipitation multiplier (XP) or temperature offset (ΔT) from modern conditions that would achieve a hydrologic balance for the palaeolake. The key difference is that the first stage of the modelling uses the geographic extent and watershed of the modern Great Salt Lake, whereas the second stage uses the larger extent of Lake Bonneville at the Bonneville or Provo levels and their associated watersheds, which were larger than the Great Salt Lake watershed. The lake area for the Bonneville level and Provo level, as well as the surface area of the Bonneville basin, are calculated from data from Oviatt (2015). To explore the range of possible P-T conditions that could have sustained Lake Bonneville, the palaeolake modelling step (e.g. stage 2) is repeated with a different temperature offset ranging from 2 to 12°C colder than modern. This offset is a constant added or subtracted to all modern monthly temperature values at every cell. Thus, the model assumes that past temperature lapse rates and seasonal patterns are the same as those observed in modern times.

Using modern CapaS, DT_lake and insolation values for the palaeolake simulation assumes that hydrologic and climatic conditions in the past were similar to those of today. To evaluate the model's sensitivity to this assumption we use 1000 Monte Carlo simulations to constrain uncertainties induced by our choice of other model parameters. Input values are drawn from a 100% (2σ) uncertainty in CapaS, DT_lake and efract, as well as a 10% (2σ) uncertainty in the evaporation coefficient *K* and insolation. Uncertainty in CapaS (soil water capacity) accounts for potential changes in vegetation and evaporative hydrology between palaeo and modern conditions. We consider 100% uncertainty to be a conservative estimate given that pollen records from the northeastern Great Basin indicate similar vegetation patterns at present and during the late Pleistocene glaciation (Thompson, 1992), providing support for the assumption that soil water capacity did not vary significantly from ~20 ka to present. Moreover, LGM records suggest that the northern Bonneville basin was dominated by sagebrush steppe with some high-elevation pine and spruce, indicating dry conditions similar to modern (Madsen *et al.*, 2001). Likewise, uncertainty in DT_Lake recognises that a deeper palaeolake may have had a different relationship with air temperature.

Finally, it is worth recognising that applying a single precipitation scale factor for all pixels changes the precipitation versus elevation gradient. However, this effect is relatively minor for two reasons. First, ~87% of annual precipitation falls within the lowest 1300 m elevation range (~1200–2500 m), reducing the impact of the largest precipitation changes across the highest elevations (~2500–3700 m) (Fig. S1). Second, the model results discussed below suggest that Lake Bonneville was likely sustained by a palaeo-precipitation increase of less than 1.25, which yields an average annual precipitation gradient of ~0.52 relative to the current lapse rate of ~0.39, in units of metres of annual precipitation per kilometre of elevation (Fig. S1). Although this is 35% steeper, it is still far less than the seasonal changes in precipitation gradient of 200 to 400% observed in the Wasatch Mountains between summer and winter months (Laabs *et al.*, 2006). To confirm a minimal impact on model results we ran an additional version of the model that uses an absolute precipitation offset for all pixels rather than a multiplier. This acts to maintain the slope of the modern precipitation-elevation gradient. Fig. S2 shows that the two models give virtually indistinguishable results.

Results

Evaporation models were trialled and selected based on their ability to reconstruct measured pan evaporation. The Abtew (1996) model is generally inaccurate at every site, likely due to its exclusion of temperature as an input. The Turc (1961) model is most accurate for Delta and Ogden, while the Condom *et al.* (2004) model performs best at Salt Lake, Provo and Logan, and also has the lowest mean SSR across all five locations (Fig. 4). During the summer months when the majority of evaporation occurs (May, June, July, August, September), the Condom model predicts evaporation in Salt Lake City with only 2.2% error. Due to its ability to accurately reproduce modern evaporation and its ease of use, the Condom evaporation model was selected for this study using a mean *K* value of 0.039 averaged across the five stations.

The first cycle of model simulations was undertaken to constrain P-T conditions during the time interval of the 'Bonneville level' when Lake Bonneville is thought to have occupied its highest shoreline elevation with no (or minimal) overflow in the millennia leading up to the Bonneville flood at ~18.2 ka (Lifton *et al.*, 2015; Oviatt and Jewell, 2016). The model yields a CapaS value of 52.3 mm with precipitation factors of roughly 1.75 and 0.94 at 2°C and 12°C temperature depressions, respectively (Fig. 5). A 10°C temperature depression generates a roughly 40% reduction in evaporation. A second model simulation constrains P-T conditions during the time interval of 'Provo abandonment', when Lake Bonneville stopped overflowing from the Provo level at ~14.8 ka (Godsey *et al.*, 2011; Oviatt, 2015). Results yield precipitation factors from 1.58 to 0.9 at 2°C and 12°C temperature depressions, respectively (Fig. 5). Because Lake Bonneville was overflowing during most of the Provo period and our model does not account for overflow, we interpret these 'Provo' results to reflect palaeoclimate conditions at *ca.* 14.8 ka as Lake Bonneville stopped overflowing and reverted to hydrologically closed conditions below the Provo shoreline (Godsey *et al.*, 2011; Oviatt, 2015).

Fig. 5 shows that uncertainty on the model variables *K*, CapaS, efract and DT_lake induce a significant spread in the modelled P-T solutions. A regression of these variable input values versus resultant precipitation factors for all Monte Carlo trials shows that the evaporation coefficient *K* has the strongest predictive power or 'weight' in the model (Fig. S3). This is not surprising given that *K* linearly modulates potential evaporation at all temperatures, such that lower values of K reduce modelled evaporation and require less precipitation to achieve a balance. A weaker predictive relationship is observed for CapaS and efract. We have also completed a suite of Monte Carlo simulations which demonstrate that using the full insolation corrections for the Provo and Bonneville intervals (2.5% or 5%, respectively) results in roughly 1% higher palaeo-precipitation estimates for Provo and roughly 2% for Bonneville (Fig. S4).

Discussion

As with water-balance modelling, glacier energy-balance modelling can be employed to reconstruct a range of

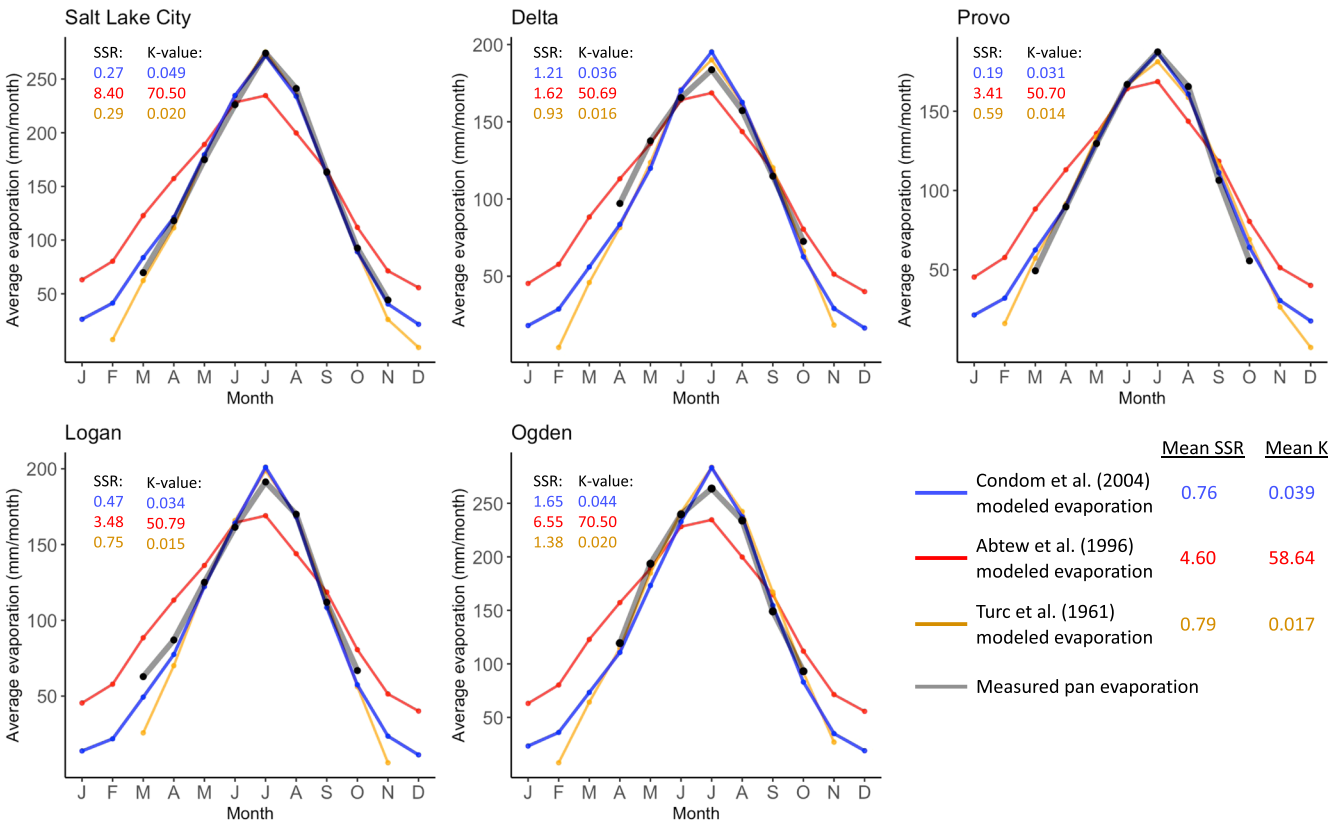

Figure 4. Comparison of Condom *et al.* (2004), Abtew (1996) and Turc (1961) evaporation model estimates with observed pan evaporation data for meteorological stations at Ogden, Delta, Salt Lake City, Logan and Provo, Utah. The minimised SSR value and optimised *K* value for each station and model are also shown. [Color figure can be viewed at wileyonlinelibrary.com]

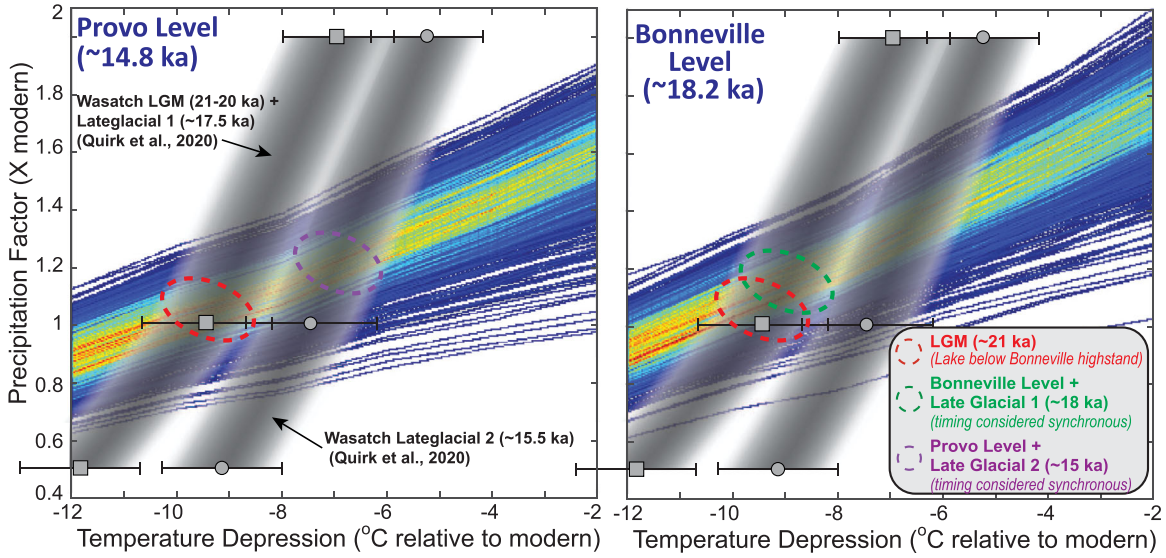

Figure 5. Model results showing the family of P-T solutions ($n = 1000$) required to achieve hydrologic balance for Lake Bonneville at the Bonneville and Provo stages (blue to red lines). Each dark blue pixel (or line) represents a single output from the Monte Carlo simulation, grading to red pixels that represent many overlapping solutions. The vertical grey bands depict modelled P-T solutions for Wasatch glacial stadials (Quirk *et al.*, 2020), with darkest grey representing the peak Gaussian uncertainty fading to transparent at the 2σ uncertainty limit. Coloured circles represent the estimated range of P-T conditions permitted within 2σ uncertainty on both the glacial and lake reconstructions during three specific time intervals discussed in the text. [Color figure can be viewed at wileyonlinelibrary.com]

palaeo-temperature and palaeo-precipitation values capable of sustaining palaeo-glaciers. Because glaciers are more sensitive to ablation-season (summer) temperature than lakes (Quirk *et al.*, 2020), glacier energy-balance models produce a set of P-T solutions exhibiting a steeper relationship than observed for lake water-balance modelling. If proximal lakes and glaciers reached known extents at the same time, the intersection of the two sets of P-T solutions can be used to more tightly constrain the range of possible P-T conditions in a region (e.g. Barth *et al.*, 2016; Ibarra *et al.*, 2018; Martin *et al.*, 2018; Plummer, 2002; Placzek, *et al.*, 2013; Quirk *et al.*, 2020).

One caveat to this method is that the mean glacier elevation is higher than the mean watershed elevation, such that the

reconstructions are based on data from different elevations. We make no correction for this issue for a few reasons. First, because both glacial and watershed temperature changes are expressed as an offset, they are directly comparable so long as temperature lapse rate remains constant. Second, precipitation is estimated as a multiplier in both cases, which our model assumes to be constant with elevation. Finally, the mean elevation of the Lake Bonneville watershed was roughly 1860 m (assuming a mean lake elevation of 1570 m), only 640 m lower than the equilibrium line altitude of Wasatch glaciers at roughly 2500 m (Laabs *et al.*, 2011).

Comparison of our results with those from a glacier-based climate reconstruction for the Wasatch Mountains (Quirk *et al.*, 2020) provides tighter constraints on palaeoclimate conditions during the 'Bonneville level' and 'Provo abandonment' intervals described above (Fig. 5). The modelled glaciers were located in several catchments across the Wasatch Range (Little Cottonwood, Big Cottonwood, Bells and Dry Creek Canyons) (Fig. 1), where three sets of moraines were built in close proximity (<5 km) to the Bonneville shoreline, defining prominent glacial stadia (Laabs *et al.*, 2011; Madsen and Currey, 1979; Quirk *et al.*, 2018; 2020). Quirk *et al.* (2020) employed cosmogenic ^{10}Be surface-exposure dating to date the abandonment of these moraines to between 21 and 20 ka (hereafter referred to as LGM), 17.5 ka (hereafter referred to as Late Glacial 1) and 15 ka (hereafter referred to as Late Glacial 2). Coupled energy mass-balance and ice-flow models (also using PRISM data as climate inputs) were used to constrain palaeoclimate conditions when each of these moraines was built (Plummer and Phillips, 2003).

To combine the glacial and lake modelling results we consider three time intervals when known lake and mountain glacier extents were most likely to overlap based on the available chronology. These include: 1) the LGM interval defined by LGM glacial maxima (~21–20 ka), when Bonneville was still rising to its overflow point; 2) the Bonneville level interval when Lake Bonneville's highest surface elevation (~18.2 ka) occurred roughly coeval with the Late Glacial 1 maxima described above (~17.5 ka), and 3) the Provo abandonment interval when Provo shoreline abandonment (~14.8 ka) was roughly coeval with the Late Glacial 2 maxima described above (~15 ka). Although climatic conditions during each interval could be satisfied by any solution along one of the four P-T lines in Fig. 5, the range of possible P-T conditions can be narrowed by recognising that specific P-T conditions must fall roughly at the intersection between two lines which represent synchronous glacial maxima and lake levels, or between two lines if it is known that the lake or glaciers occupied some intermediate extent at that time. The coloured ovals in Fig. 5 show our best estimate of P-T conditions during each interval by capturing the overlapping 2σ uncertainty on both the glacial and lake reconstructions.

For example, at the first LGM interval (21–20 ka) it can be assumed that conditions fell along the LGM glacier solutions between the Bonneville level and Provo lake solutions because the size of Lake Bonneville was larger than Provo but had not yet reached the overflow point (Oviatt, 2015). As illustrated by the red oval in Fig. 5, this position centres on a temperature depression of roughly -9°C and a 7% increase in precipitation relative to modern. Conditions during the second Bonneville level interval (~18.2–17.5 ka), must have fallen near the intersection of the Bonneville level solutions and the LGM/Late Glacial 1 solutions, given that these two events are taken to be synchronous (Quirk *et al.*, 2020). The green oval in Fig. 5 delineates the interval, suggesting a temperature depression of roughly -9°C and 16% higher precipitation. Finally, for the Provo abandonment interval (~15–14.8 ka), we expect P-T conditions to fall at the

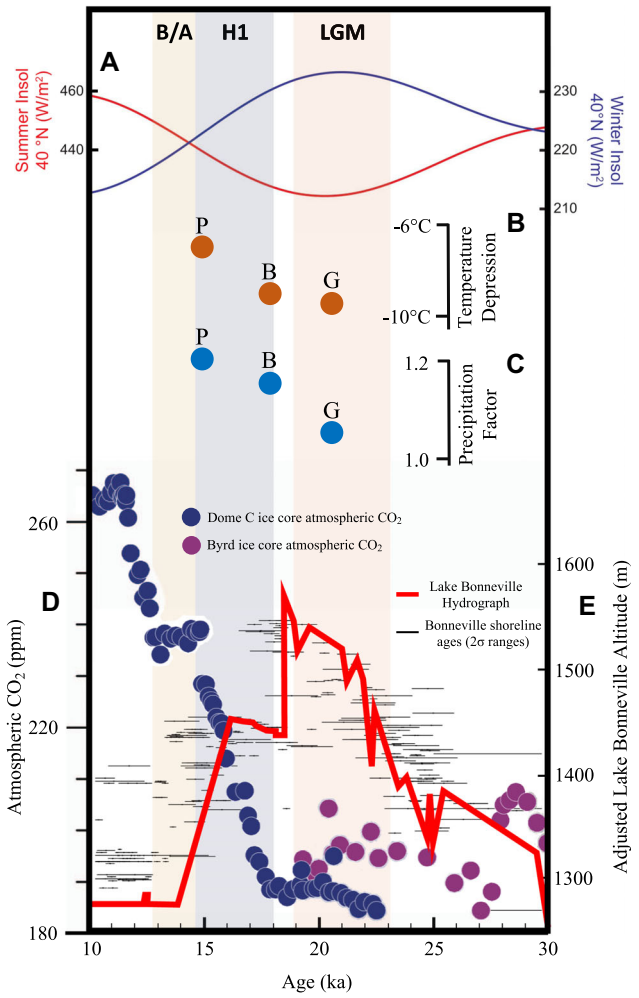

Figure 6. Adapted from Ibarra *et al.* (2014) and Clark *et al.* (2009). (A) Insolation data from Laskar *et al.* (2004). (B) Temperature depressions (°C) and (C) precipitation factors (with respect to modern) that sustained hydrologic balance for Lake Bonneville (this study), G = LGM, B = Bonneville level, P = Provo abandonment. (D) Atmospheric CO_2 from the Dome C ice core (purple circles) from Ahn *et al.* (2004) and Byrd ice core (blue circles) from Ahn *et al.* (2008). (E) Lake Bonneville hydrograph from Oviatt (2015). [Color figure can be viewed at wileyonlinelibrary.com]

intersection of the Provo and Late Glacial 2 lines (Godsey *et al.*, 2011; Quirk *et al.*, 2020). The purple oval in Fig. 5 thus suggests a roughly -7°C temperature depression and a roughly 21% precipitation increase at this time.

A major finding of this work is that Lake Bonneville's level at the LGM only required a roughly 7% increase in precipitation, suggesting lake expansion was primarily driven by colder temperatures that suppressed evaporation. We thus propose that the Bonneville transgression and broadly synchronous LGM highstands in lakes Franklin, Clover and Surprise, located farther west in the Great Basin, occurred as the region passed through a climatic optimum in which the return of relatively modest wetness combined with still heavily depressed temperatures to create a positive hydrologic budget (Ibarra *et al.*, 2014; Munroe and Laabs, 2013b). This idea agrees well with the results of Ibarra *et al.* (2014), who concluded that the late-LGM transgression (~22–19 ka) of Lake Surprise was driven by only a 10% increase in palaeo-precipitation and a ~36% reduction in evaporation rate in northeasternmost California. It also agrees well with conclusions independently reached by Quirk *et al.* (2020) and with TraCE-21 ka climate simulation results showing dry conditions during the LGM (He, 2011; Ivanovic *et al.*, 2016; Liu *et al.*, 2009). Individual

climate models from the Paleoclimate Model Intercomparison Project 3, which show best agreement with the proxy record at 21 ka, also show minimal increases in precipitation compared with modern times (Ibarra *et al.*, 2019; Oster *et al.*, 2015).

The role of colder temperatures in driving pluvial lake transgression during the LGM interval (~21–20 ka) is also supported by a maximum in winter insolation and minimum summer insolation at 40° north from ~22 to 18.5 ka (Laskar *et al.*, 2004), along with decreased CO_2 levels (Shakun *et al.*, 2012). Fig. 6 demonstrates the synchronicity of Lake Bonneville's LGM transgression and highest lake level with decreased CO_2 levels, decreased summer insolation, and cooler and drier conditions in the Bonneville basin, supporting the idea that increased precipitation was not fundamental in driving lakes to highstands at this time. A focus on the importance of temperature instead of precipitation as a driving factor in LGM highstands contrasts with some traditional precipitation-focused explanations for pluvial lake transgressions (Antevs 1948; Benson and Thompson, 1987; Hostetler and Benson 1990; Bartlein *et al.*, 1998), including the idea of multiple north–south oscillations of the Pacific Jet Stream (Munroe and Laabs, 2013b), and an 'out of the tropics' model in which moisture is sourced from the south (Lyle *et al.*, 2012).

Further support for cool conditions in the Bonneville basin at this time comes from proxies such as amino-acid palaeothermometry performed on ostracode shells from Lake Bonneville, indicating that temperatures were 8.3 ± 3°C colder during the LGM than modern (Kaufman, 2003). Palaeovegetation records developed largely from packrat middens in the Lake Bonneville basin also indicate significant cooling during the interval when the lake expanded and while it overflowed (Rhode, 2016 and references therein).

Precipitation seems to have increased to roughly 16% above modern by the time of the Bonneville level (*ca.* 18.2–17.5 ka) and to roughly 21% by the time of Provo abandonment (*ca.* 15–14.8 ka). This suggests that wetter conditions may have prevailed throughout much of the Heinrich I (H1) event from ~17.2 to 15 ka, when many lakes reached their ultimate highstands of the last pluvial cycle, including: Lake Clover at ~17 ka (Munroe *et al.*, 2020), Jakes Lake at ~16.8 ka (Barth *et al.*, 2016) and Lake Franklin at ~16.5 ka (Munroe and Laabs, 2013a), followed by the more western Lake Lahontan at ~15.8 ka (Matsubara and Howard, 2009) and northwestern Lake Surprise at ~15.2 ka (Ibarra *et al.*, 2014) (Fig. 7). Ibarra *et al.* (2014) provide support for increased precipitation, estimating that a roughly 70% increase in precipitation from modern was required to grow Lake Surprise to its highstand at *ca.* 15.2 ka. Likewise, in the southern Great Basin, the Pinnacle Cave record shows cold conditions centred at 18.6 ka, followed by rapid warming and wetting associated with H1 (Lachniet *et al.*, 2011). Increased precipitation during H1 has been attributed to a southward shift in the thermal equator and a strengthened, equatorward-shifted westerly storm track during H1 (Broecker and Putnam, 2013; Hudson *et al.*, 2019), driven by teleconnections with the cooling North Atlantic (McManus *et al.*, 2004; Bard *et al.*, 2000; Okumura *et al.*, 2009).

Although the above results suggest relatively wet conditions until about 15 ka, many records from the southwestern United States suggest a transition from wetter to drier conditions beginning between about 15.5 and 14.5 ka, roughly coincident with the end of the H1 period (Asmerom *et al.*, 2010; Polyak *et al.*, 2012; Wagner *et al.*, 2010). In Arizona, oxygen isotope data from the Cave of the Bells indicate a deglacial transition and increased aridity beginning around 15.3 ka, attributed to a northward shift of the thermal equator, a poleward-shifted storm track and weakening of the Aleutian Low (Broecker and Putnam, 2013; Hudson *et al.*, 2019; Wagner *et al.*, 2010). If correct, a northward-shifted storm track could have contributed to enhanced wetness at Lake Bonneville, Lake Surprise (Ibarra *et al.*, 2014) and Lake Chewaucan (Hudson *et al.*, 2019) until *ca.* 15 ka, while Arizona became increasingly arid. In New Mexico, stable isotope records from Fort Stanton Cave speleothems suggest a wetter H1, followed by rapid drying beginning around 14.5 ka (Asmerom *et al.*, 2010; Polyak *et al.*, 2012). At Pinnacle Cave, speleothem growth halted at *ca.* 15.6 ka,

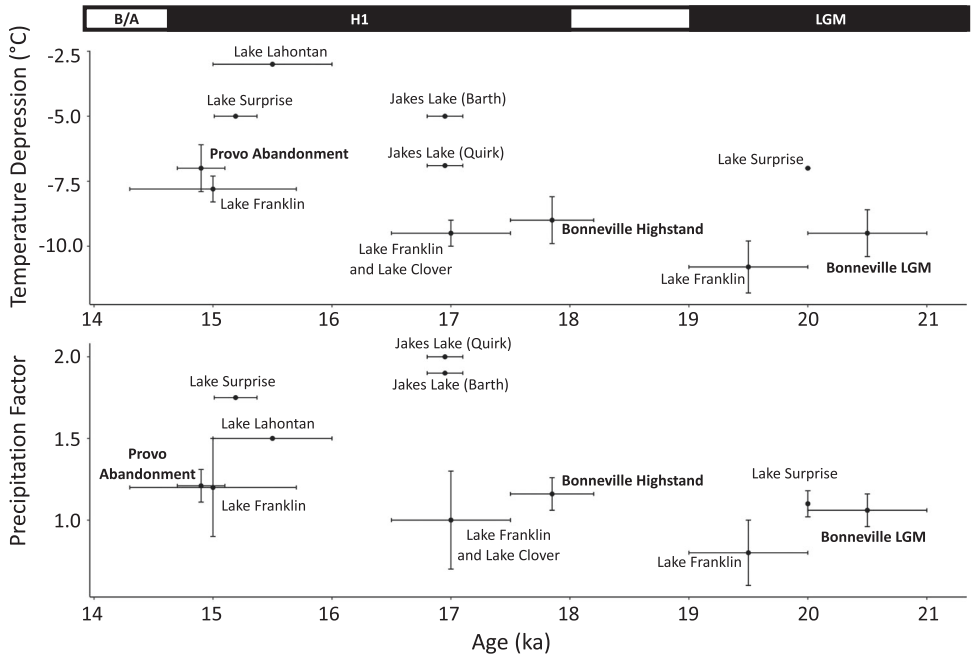

Figure 7. Precipitation factors and temperature depressions (in °C) required to sustain pluvial lake relative highstands during the late-Last Glacial Maximum (LGM) and Heinrich Stadial 1 (H1). Lake Bonneville data are from this study. Lake Lahontan data from Matsubara and Howard (2009), Lake Surprise from Ibarra *et al.* (2014), Jakes Lake from Barth *et al.* (2016) and Quirk *et al.* (2018) and ages from García and Stokes (2006), Lake Clover and Lake Franklin data from Dahle (2021).

possibly due to decreased precipitation related to the poleward-shifted storm track during the onset of the Bølling–Allerød (Lachniet *et al.*, 2011). Charcoal data from Marlon *et al.*, (2009) suggest that this drying was widespread across the entire southwestern United States after H1, including the Bonneville basin. Finally, regression of Lakes Lahontan (Benson *et al.*, 1995; Adams *et al.*, 2008), Franklin (Munroe and Laabs, 2013a), Clover (Munroe *et al.*, 2020) and Surprise (Ibarra *et al.*, 2014) and Bonneville itself after ~15 ka provide further support for a return to drier conditions following H1 in the southern Great Basin, while the northwestern United States experienced peak wet conditions during this period (Hudson *et al.*, 2019).

Drying in the southern Great Basin synchronous with wetting in the greater Pacific Northwest after H1 has been tied to modern precipitation dynamics and future projections of water availability (e.g. Broecker and Putnam, 2013). Hudson *et al.* (2019) note numerous pollen and diatom assemblages from Oregon that evidence a wetter Bølling–Allerød (14.6–12.8 ka) relative to H1, providing support for a north–south precipitation dipole pattern controlled by the relative strength and position of the winter storm track during the deglacial period. Modern winter hydroclimate in the western United States has been shown to follow a similar pattern on interannual to decadal timescales, with wet winters in the southwest corresponding to dry winters in the northwest, and vice versa (e.g. Hudson *et al.*, 2019; Lins, 1997; Redmond, 1991). Northern Hemisphere warming and sea ice loss associated with anthropogenic climate change is expected to shift the thermal equator northward (Broecker and Putnam, 2013), leading to a strengthened dry-SW/wet-NW mean state and drier conditions throughout the Great Basin with future warming.

Conclusions

This study uses the hydrologic balance model of Condom *et al.* (2004) to evaluate the range of precipitation and temperature conditions required to sustain Lake Bonneville at the moment it began to overflow from its highest shoreline (*ca.* 18.2 ka) and again at the moment it dropped below its overflow threshold at the Provo shoreline (*ca.* 14.8 ka). Intersecting these P-T solution curves with steeper P-T curves derived from modelling glacial maxima in the nearby Wasatch Mountains more tightly constrains P-T conditions for three time intervals. Results suggest that the region was cold and dry during the LGM, after which precipitation increased gradually until roughly 15 ka. Specifically, during the LGM interval (~21–20 ka) Lake Bonneville was able to approach its highest water level under conditions roughly 9.5°C colder but only 7% wetter than today. We thus propose that LGM highstands in regional lakes such as Franklin, Clover, Surprise and Bonneville were not caused by large increases in precipitation, but rather by a climatic optimum in which moderate wetness coupled with greatly depressed temperatures to create positive hydrologic budgets. The Bonneville level itself (~18.2–17.5 ka) resulted from roughly 16% higher precipitation and temperatures roughly 9°C lower than today. This result is consistent with the many regional lake highstands that occurred from *ca.* 17 to 15 ka, which collectively signal increasingly wet conditions. Our modelling of the Provo abandonment interval (*ca.* 15–14.8 ka) suggests that the shrinking of Lake Bonneville below the Provo level was driven primarily by roughly 2°C of warming relative to the Bonneville level, which offset increasingly wet conditions with precipitation roughly 21% higher than modern. Increasing aridity led to a rapid decline from the Provo level after 15 ka. The hydrologic balance-model results from this study reveal that cold conditions drove dramatic hydroclimate shifts during the LGM, demonstrating the role of temperature fluctuations in controlling water availability across the Great Basin and southwestern United States.

Acknowledgements and funding. This work was funded by NSF grant EAR-1702975 to W. Amidon and J. Munroe and EAR-1702898 to B. Laabs, obtained through the P2C2 program. We acknowledge Jessica Oster and Dan Ibarra for discussion and input. The detailed comments of three anonymous reviewers improved the manuscript considerably.

Conflict of interest statement—The authors declare that they have no known competing financial interests or personal relationships that could have appeared to influence the work reported in the paper.

Authorship and authors contributions

Project ideas and funding obtained by WHA, BJCL and JSM. Modelling completed by BKB and WHA. Paper written primarily by BKB and WHA. Significant intellectual contributions by all authors.

Supporting information

Additional supporting information can be found in the online version of this article.

Figure S1. A) Cumulative precipitation as a function of elevation. Notice that relatively little total precipitation comes from the higher elevations given their comparatively small area. Precipitation data source: PRISM Group. B) Modern precipitation–elevation gradient in the Lake Bonneville basin. C) Temperature as a function of cumulative area. Notice that most of the study area has a mean annual temperature less than 6°C. Temperature data source: PRISM Group. D) Modern temperature lapse rate in the Lake Bonneville basin.

Figure S2. Comparison of Monte Carlo results demonstrating that similar results are obtained when the model solves for palaeo-precipitation as a multiple of modern (first column) as when it solves for palaeo-precipitation as an absolute offset from modern (middle and right hand columns). The absolute offset approach applies the same increase or decrease to all pixels for all months, thereby preserving the modern elevation–precipitation gradient.

Figure S3. Correlations between various input variables (*K*, CapaS, efract and DT Lake) and the mean precipitation multiplier. Each dot represents an individual Monte Carlo simulation for which random unique input values were chosen. The evaporation coefficient *K* has the largest impact on palaeo-precipitation followed by CapaS and efract.

Figure S4. Comparison of Monte Carlo results demonstrating that similar results are obtained for models simulated using modern insolation values instead of insolation values adjusted according to the predictions of Laskar *et al.*, 2004.

References

Abtew W. 1996. Evapotranspiration measurement and modeling for three wetland systems in South Florida. *Water Resources Bulletin* **32**: 465–473.

Adams KD, Goebel T, Graf K *et al.* 2008. Late Pleistocene and early Holocene lake-level fluctuations in the Lahontan Basin, Nevada: Implications for the distribution of archaeological sites. *Geoarchaeology* **23**(5): 608–643.

Ahn J, Brook EJ. 2008. Atmospheric CO_2 and climate on millennial time scales during the last glacial period. *Science* **322**(5898): 83–85.

Ahn J, Wahlen M, Deck BL *et al.* 2004. A record of atmospheric CO_2 during the last 40,000 years from the Siple Dome, Antarctica ice core. *Journal of Geophysical Research: Atmospheres* **109**(D13). http://doi.org/10.1029/2003jd004415

Antevs E. 1948. *The Great Basin, with Emphasis on Glacial and Postglacial Times: Climatic Changes and Pre-white Man. III*. University of Utah.

Asmerom Y, Polyak VJ, Burns SJ. 2010. Variable winter moisture in the southwestern United States linked to rapid glacial climate shifts. *Nature Geoscience* **3**: 114–117.

Bard E, Rostek F, Turon JL *et al.* 2000. Hydrological impact of Heinrich events in the subtropical northeast Atlantic. *Science* **289**(5483): 1321–1324.

Barth C, Boyle DP, Hatchett BJ *et al.* 2016. Late Pleistocene climate inferences from a water balance model of Jakes Valley, Nevada (USA). *Journal of Paleolimnology* **56**(2–3): 109–122.

Bartlein PJ, Anderson KH, Anderson PM *et al.* 1998. Paleoclimate simulations for North America over the past 21,000 years: features of the simulated climate and comparisons with paleoenvironmental data. *Quaternary Science Reviews* **17**(6–7): 549–585.

Belovsky GE, Stephens D, Perschon C *et al.* 2011. The Great Salt Lake Ecosystem (Utah, USA): long term data and a structural equation approach. *Ecosphere* **2**(3): 1–40.

Benson LV, Thompson RS. 1987. Lake-level variation in the Lahontan Basin for the past 50,000 years. *Quaternary Research* **28**(1): 69–85.

Benson LV, Currey DR, Dorn RI *et al.* 1990. Chronology of expansion and contraction of four Great Basin lake systems during the past 35,000 years. *Palaeogeography, Palaeoclimatology, Palaeoecology* **78**(3–4): 241–286.

Benson L, Kashgarian M, Rubin M. 1995. Carbonate deposition, Pyramid Lake subbasin, Nevada: 2. Lake levels and polar jet stream positions reconstructed from radiocarbon ages and elevations of carbonates (tufas) deposited in the Lahontan basin. *Palaeogeography, Palaeoclimatology, Palaeoecology* **117**(1–2): 1–30.

Benson LV, Lund SP, Smoot JP *et al.* 2011. The rise and fall of Lake Bonneville between 45 and 10.5 ka. *Quaternary International* **235**(1–2): 57–69.

Broecker WS, Kaufman A. 1965. Radiocarbon chronology of Lake Lahontan and Lake Bonneville II, Great Basin. *Geological Society of America Bulletin* **76**(5): 537–566.

Broecker WS, Putnam AE. 2013. Hydrologic impacts of past shifts of Earth's thermal equator offer insight into those to be produced by fossil fuel CO_2. *Proceedings of the National Academy of Sciences* **110**(42): 16710–16715.

Clark PU, Dyke AS, Shakun JD *et al.* 2009. The last glacial maximum. *Science* **325**(5941): 710–714.

Condom T, Coudrain A, Dezetter A *et al.* 2004. Transient Modelling of lacustrine regressions: two case studies from the Andean Altiplano. *Hydrological Processes* **18**: 2395–2408.

Cook BI, Ault TR, Smerdon JE. 2015. Unprecedented 21st century drought risk in the American Southwest and Central Plains. *Science Advances* **1**(1). http://doi.org/10.1126/sciadv.1400082

Cook BI, Mankin JS, Marvel K *et al.* 2020. Twenty-First Century Drought Projections in the CMIP6 Forcing Scenarios. *Earth's Future* **8**(6). http://doi.org/10.1029/2019ef001461

Currey DR, Oviatt CG. 1985. Durations, average rates, and probable causes of Lake Bonneville expansions, stillstands, and contractions during the last deep lake cycle, 32 to 10,000 years ago. In *Problems of and Prospects for Predicting Great Salt Lake Levels*, Kay PA, Diaz HF (eds). University of Utah Center for Public Affairs and Administration: Salt Lake City; 9–24.

Currey DR. 1990. Quaternary palaeolakes in the evolution of semidesert basins, with special emphasis on Lake Bonneville and the Great Basin, U.S.A. *Palaeogeography, Palaeoclimatology, Palaeoecology* **76**: 189–214.

Dahle JR. 2021. *Late Quaternary Glacier and Climate Change in the Northeastern Great Basin* (Masters dissertation, North Dakota State University).

Fick SE, Hijmans RJ. 2017. WorldClim 2: new 1-km spatial resolution climate surfaces for global land areas. *International Journal of Climatology* **37**(12): 4302–4315.

García AF, Stokes M. 2006. Late Pleistocene highstand and recession of a small, high-altitude pluvial lake, Jakes Valley, central Great Basin, USA. *Quaternary Research* **65**(1): 179–186.

Gilbert GK. 1890. *Lake Bonneville* (**1**). US Government Printing Office

Godsey HS, Currey DR, Chan MA. 2005. New evidence for an extended occupation of the Provo shoreline and implications for regional climate change, Pleistocene Lake Bonneville, Utah, USA. *Quaternary Research* **63**(2): 212–223.

Godsey HS, Oviatt CG, Miller DM *et al.* 2011. Stratigraphy and chronology of offshore to nearshore deposits associated with the Provo shoreline, Pleistocene Lake Bonneville, Utah. *Palaeogeography, Palaeoclimatology, Palaeoecology* **310**(3–4): 442–450.

Hatchett BJ. 2018. Fingerprints of the thermal equator. *Nature Geoscience* **11**(6): 387.

Hargreaves GH. 1975. Moisture availability and crop production. *Transactions of the ASAE* **18**(5): 980–984.

He F. 2011. *Simulating Transient Climate Evolution of the Last Deglaciation with CCSM3*. Ph.D thesis. Department of Atmospheric and Oceanic Sciences, University of Wisconsin-Madison.

Hostetler S, Benson LV. 1990. Paleoclimatic implications of the high stand of Lake Lahontan derived from models of evaporation and lake level. *Climate Dynamics* **4**(3): 207–217.

Hostetler SW, Giorgi F, Bates GT *et al.* 1994. Lake-atmosphere feedbacks associated with paleolakes Bonneville and Lahontan. *Science* **263**(5147): 665–668.

Hudson AM, Hatchett BJ, Quade J *et al.* 2019. North-south dipole in winter hydroclimate in the western United States during the last deglaciation. *Scientific reports* **9**(1): 1–12.

Ibarra DE, Egger AE, Weaver KL *et al.* 2014. Rise and fall of late Pleistocene pluvial lakes in response to reduced evaporation and precipitation: Evidence from Lake Surprise. *California. GSA Bulletin* **126**(11–12): 1387–1415.

Ibarra DE, Oster JL, Winnick MJ *et al.* 2018. Warm and cold wet states in the western United States during the Pliocene–Pleistocene. *Geology* **46**(4): 355–358.

Ibarra DE, Oster JL, Winnick MJ *et al.* 2019. Lake area constraints on past hydroclimate in the western United States: Application to Pleistocene Lake Bonneville. *Utah Geological Survey Miscellaneous Publication* **170**: 6.

Ivanovic RF, Gregoire LJ, Kageyama M *et al.* 2016. Transient climate simulations of the deglaciation 21–9 thousand years before present (version 1)–PMIP4 Core experiment design and boundary conditions. *Geoscientific Model Development* **9**(7): 2563–2587.

Kaufman DS. 2003. Amino acid paleothermometry of Quaternary ostracodes from the Bonneville Basin, Utah. *Quaternary Science Reviews* **22**(8–9): 899–914.

Laabs BJC, Plummer MA, Mickelson DM. 2006. Climate during the last glacial maximum in the Wasatch and southern Uinta Mountains inferred from glacier modeling. *Geomorphology* **75**(3–4): 300–317.

Laabs BJC, Marchetti DW, Munroe JS *et al.* 2011. Chronology of latest Pleistocene mountain glaciation in the western Wasatch Mountains, Utah, USA. *Quaternary Research* **76**(2): 272–284.

Lachniet MS, Asmerom Y, Polyak V. 2011. Deglacial paleoclimate in the southwestern United States: an abrupt 18.6 ka cold event and evidence for a North Atlantic forcing of Termination I. *Quaternary Science Reviews* **30**(27–28): 3803–3811.

Laskar J, Robutel P, Joutel F *et al.* 2004. A long-term numerical solution for the insolation quantities of the Earth. *Astronomy & Astrophysics* **428**(1): 261–285.

Lifton N, Caffee M, Finkel R *et al.* 2015. In situ cosmogenic nuclide production rate calibration for the CRONUS-Earth project from Lake Bonneville, Utah, shoreline features. *Quaternary Geochronology* **26**: 56–69.

Lins HF. 1997. Regional streamflow regimes and hydroclimatology of the United States. *Water Resources Research* **33**(7): 1655–1667.

Liu Z, Otto-Bliesner BL, He F *et al.* 2009. Transient simulation of last deglaciation with a new mechanism for Bølling-Allerød warming. *Science* **325**(5938): 310–314.

Lyle M, Heusser L, Ravel C *et al*. 2012. Out of the Tropics: The Pacific, Great Basin Lakes, and Late Pleistocene Water Cycle in the Western United States. *Science* **337**: 1629–1633.

Madsen DB, Currey DR. 1979. Late Quaternary glacial and vegetation changes, Little Cottonwood Canyon area, Wasatch Mountains, Utah, *Quaternary Research*. **12**(2): 254–270.

Madsen DB, Rhode D, Grayson DK *et al*. 2001. Late Quaternary environmental change in the Bonneville basin, western USA. *Palaeogeography, Palaeoclimatology, Palaeoecology* **167**(3–4): 243–271.

Marlon JR, Bartlein PJ, Walsh MK *et al*. 2009. Wildfire responses to abrupt climate change in North America. *Proceedings of the National Academy of Sciences* **106**(8): 2519–2524.

Martin LC, Blard PH, Lavé J *et al*. 2018. Lake Tauca highstand (Heinrich Stadial 1a) driven by a southward shift of the Bolivian High. *Science Advances* **4**(8): eaar2514.

Matsubara Y, Howard AD. 2009. A spatially explicit model of runoff, evaporation, and lake extent: Application to modern and late Pleistocene lakes in the Great Basin region, western United States. *Water Resources Research* **45**(6): W06425.

McGee D, Quade J, Edwards RL *et al*. 2012. Lacustrine cave carbonates: Novel archives of paleohydrologic change in the Bonneville Basin (Utah, USA). *Earth and Planetary Science Letters* **351**: 182–194.

McManus JF, Francois R, Gherardi JM *et al*. 2004. Collapse and rapid resumption of Atlantic meridional circulation linked to deglacial climate changes. *Nature* **428**(6985): 834–837.

Miller DM, Oviatt CG, Nash BP. 2008. Late Pleistocene Hansel Valley basaltic ash, northern Lake Bonneville, Utah, USA. *Quaternary International* **178**(1): 238–245.

Miller DM, Oviatt CG, Mcgeehin JP. 2013. Stratigraphy and chronology of Provo shoreline deposits and lake-level implications, Late Pleistocene Lake Bonneville, eastern Great Basin, USA. *Boreas* **42**(2): 342–361.

Miller DM. 2016. The Provo shoreline of Lake Bonneville, *Developments in Earth Surface Processes* **20**: 127–144. Elsevier.

Munroe JS, Laabs BJC. 2013a. Latest Pleistocene history of pluvial Lake Franklin, northeastern Nevada, USA. *GSA Bulletin* **125**(3–4): 322–342.

Munroe JS, Laabs BJC. 2013b. Temporal correspondence between pluvial lake highstands in the southwestern US and Heinrich Event 1. *Journal of Quaternary Science* **28**(1): 49–58.

Munroe JS, Walcott CK, Amidon WH *et al*. 2020. A top-to-bottom luminescence-based chronology for the post-LGM regression of a Great Basin pluvial Lake. *Quaternary* **3**(2): 11.

O'Connor JE. 1993. *Hydrology, hydraulics, and geomorphology of the Bonneville flood* (**274**). Geological Society of America.

O'Connor J. 2016. The Bonneville flood—a veritable Débâcle, *Developments in Earth Surface Processes* **20**: 105–126. Elsevier.

Okumura YM, Deser C, Hu A *et al*. 2009. North Pacific climate response to freshwater forcing in the subarctic North Atlantic: Oceanic and atmospheric pathways. *Journal of Climate* **22**(6): 1424–1445.

Oster JL, Ibarra DE, Winnick MJ *et al*. 2015. Steering of westerly storms over western North America at the Last Glacial Maximum. *Nature Geoscience* **8**(3): 201.

Oviatt CG. 1997. Lake Bonneville fluctuations and global climate change. *Geology* **25**(2): 155–158.

Oviatt CG. 2015. Chronology of Lake Bonneville, 30,000 to 10,000 yr BP. *QuaternaryScience Reviews* **110**: 166–171.

Oviatt CG, Currey DR, Miller DM. 1990. Age and paleoclimatic significance of the stansbury shoreline of Lake Bonneville, Northeastern Great Basin. *Quaternary Research* **33**(3): 291–305.

Oviatt CG, Jewell PW. 2016. The Bonneville Shoreline: Reconsidering Gilbert's Interpretation, *In Developments in Earth Surface Processes* **20**: 88–104. Elsevier.

Oviatt CG, Nash WP. 1989. Late Pleistocene basaltic ash and volcanic eruptions in the Bonneville basin, Utah. *Geological Society of America Bulletin* **101**(2): 292–303.

Oviatt CG, Nash BP. 2014. The Pony Express Basaltic Ash: a Stratigraphic Marker in Late Pleistocene Lake Bonneville Deposits. *Utah. Utah Geological Survey Miscellaneous Publication* **14**: 1.

Pack FJ. 1939. Lake Bonneville: A popular treatise dealing with the history and physical aspects of Lake Bonneville, *Bulletin of the University of Utah*. **30**(4): 112.

Placzek CJ, Quade J, Patchett PJ. 2013. A 130 ka reconstruction of rainfall on the Bolivian Altiplano. *Earth and Planetary Science Letters* **363**: 97–108.

Plummer MA. 2002. Paleoclimatic Conditions during the Last Deglaciation Inferred from Combined Analysis of Pluvial and Glacial Records: A Paleohydrology Study of the Owns Valley, California [Ph.D. thesis]. New Mexico Institute of Mining and Technology. 346.

Plummer MA, Phillips FM. 2003. A 2-D numerical model of snow/ice energy balance and ice flow for paleoclimatic interpretation of glacial geomorphic features. *Quaternary Science Reviews* **22**(14): 1389–1406.

Polyak VJ, Asmerom Y, Burns SJ *et al*. 2012. Climatic backdrop to the terminal Pleistocene extinction of North American mammals. *Geology* **40**(11): 1023–1026.

Quirk BJ, Moore JR, Laabs BJC *et al*. 2018. Termination II, Last Glacial Maximum, and Lateglacial chronologies and paleoclimate from Big Cottonwood Canyon, Wasatch Mountains, Utah. *GSA Bulletin* **130**(11–12): 1889–1902.

Quirk BJ, Moore JR, Laabs BJC *et al*. 2020. Latest Pleistocene glacial and climate history of the Wasatch Range, Utah. *Quaternary Science Reviews* **238**: 106313.

Redmond KT, Koch RW. 1991. Surface climate and streamflow variability in the Western United States and their relationship to large-scale circulation indices. *Water Resources Research* **27**(9): 2381–2399.

Reheis MC. 1999. Extent of Pleistocene Lakes in the Western Great Basin: USGS Miscellaneous Field Studies Map MF-2323, U.S. Geological Survey, Denver, CO.

Rhode D. 2016. Quaternary vegetation changes in the Bonneville basin, *Developments in Earth Surface Processes* **20**: 420–441. Elsevier.

Scott WE, McCoy WD, Shroba RR *et al*. 1983. Reinterpretation of the exposed record of the last two cycles of Lake Bonneville, western United States. *Quaternary Research* **20**(3): 261–285.

Seager R, Vecchi GA. 2010. Greenhouse warming and the 21st century hydroclimate of southwestern North America. *Proceedings of the National Academy of Sciences* **107**(50): 21277–21282.

Sengupta M, Xie Y, Lopez A *et al*. 2018. The national solar radiation data base (NSRDB). *Renewable and Sustainable Energy Reviews* **89**: 51–60.

Shakun JD, Clark PU, He F *et al*. 2012. Global warming preceded by increasing carbon dioxide concentrations during the last deglaciation. *Nature* **484**(7392): 49–54.

Task Committee on Hydrology Handbook of Management Group D of ASCE. 1996. *Hydrology handbook*. American Society of Civil Engineers.

Thompson RS. 1992. Late Quaternary environments in Ruby Valley, Nevada. *Quaternary Research* **37**(1): 1–15.

Turc L. 1961. Estimation of irrigation water requirements, potential evapotranspiration: a simple climatic formula evolved up to date. *Annales Agronomiques* **12**(1): 13–49.

Wagner JD, Cole JE, Beck JW *et al*. 2010. Moisture variability in the southwestern United States linked to abrupt glacial climate change. *Nature Geoscience* **3**(2): 110–113.

Western Regional Climate Center. 2019. Cooperative Climatological Data Summaries, Pan Evaporation. Retrieved from: https://wrcc.dri.edu/Climate/comp_table_show.php?stype=pan_evap_avg

White JS, Null SE, Tarboton DG. 2014. *Modeled changes to Great Salt Lake salinity from railroad causeway alteration*. Final Report to the Utah Division of Forestry, Fire and State Lands.

Williams JS. 1952. Red Rock Pass, outlet of Lake Bonneville. *Geological Society of America Bulletin* **63**(12): 1375.

Xu CY, Singh VP. 2000. Evaluation and generalization of radiation-based methods for calculating evaporation. *Hydrological processes* **14**(2): 339–349.